Molecular & Biochemical Parasitology 248 (2022) 111463

Contents lists available at ScienceDirect

Molecular & Biochemical Parasitology

journal homepage: www.elsevier.com/locate/molbiopara

The essential cysteines in the CIPC motif of the thioredoxin-like *Trypanosoma brucei* MICOS subunit TbMic20 do not form an intramolecular disulfide bridge *in vivo*

Iosif Kaurov [a], Jiří Heller [a], Sebastian Deisenhammer [b], David Potěšil [c], Zbyněk Zdráhal [c], Hassan Hashimi [a,b,*]

[a] Institute of Parasitology, Biology Center, Czech Academy of Sciences, 37005 České Budějovice, Czech Republic
[b] Faculty of Science, University of South Bohemia, 37005 České Budějovice, Czech Republic
[c] Central European Institute of Technology, Masaryk University, 62500 Brno, Czech Republic

ARTICLE INFO

Keywords:
Trypanosoma
Mitochondrion
MICOS
Protein import
Intermembrane space
Oxidative folding

ABSTRACT

The mitochondrial protein import machinery of trypanosomatids is highly divergent from that of the well-studied models such as baker's yeast. A notable example is that the central catalyst of the mitochondrial intermembrane space import and assembly pathway (MIA), named Mia40, is missing in trypanosomatids. Mia40 works in a two-step process. First it recognizes by direct binding reduced MIA substrate proteins and then catalyzes their oxidative folding to produce intramolecular disulfide bridges. It was recently proposed that a thioredoxin-like subunit of the trypanosomal mitochondrial contact site and cristae organizing system (MICOS) called TbMic20 may be the Mia40 replacement. Our study performed on procyclic stage of the parasite revealed that each of the two cysteines in TbMic20′s active site is essential for the stability of MIA substrate proteins although they do not form a disulfide bridge *in vivo*. The two cysteines of Mia40′s active site form an intramolecular disulfide bridge at steady state, which is a prerequisite for its oxidative folding of MIA substrates. Thus, we conclude that TbMic20 is unlikely to represent a *bona fide* Mia40 replacement and plays a still unresolved role in the stability and/or import of MIA substrates in trypanosomatids. Despite this, the effect of TbMic20 depletion and mutation indicates that the trypanosomal MICOS complex still plays a vital role in the maturation and/or stability of proteins imported by the MIA pathway.

1. Introduction

Mitochondria are protein-rich organelles. Nevertheless, only a small portion of mitochondrial proteins are synthesized within the organelle from a handful of genes encoded in reduced mitochondrial genomes. The majority is translated in the cytosol and imported into the mitochondrion [1]. Thus, protein import into mitochondria is essential. Proteins mostly enter mitochondria through translocase of the outer membrane complex. Further distribution between different mitochondrial compartments is defined by a combination of targeting sequences and is performed by several sorting and import machineries.

A significant portion of intermembrane space (IMS) proteins goes through the mitochondrial intermembrane space import and assembly (MIA) pathway [2–4]. MIA substrates are usually small proteins less than 20 kDa, containing cysteine residues, typically organized in twin C (X3)C or C(X9)C motifs. C(X3)C motifs are common for small translocase of the inner membrane (TIM) proteins [5]. IMS protein folding starts by recognition of the substrate by the core MIA enzyme Mia40 [6,7]. The IMS-targeting signal (ITS) or mitochondria IMS-sorting signal (MISS) sequence on the freshly imported protein binds to the receptor, a hydrophobic cleft formed by Mia40′s own twin C(X9)C motif [8]. This allows proper positioning of the substrate so that covalent

Abbreviations: AMS, 4-acetamido-4-maleimidylstilbene-2,2-disulfonic acid; Dox, doxycycline; DTT, DL-Dithiothreitol; GSH, reduced glutathione; GSSG, glutathione disulfide; IAA, Iodoacetamide; IMS, intermembrane space; ITS, IMS-targeting signal; MIA, mitochondrial intermembrane space import and assembly pathway; MICOS, mitochondrial contact site and cristae organizing system; MISS, mitochondria IMS-sorting signal, NEM, N-ethylmaleimide; PDI, protein disulfide isomerase; ROS, reactive oxygen species; TCA, trichloroacetic acid; TCEP, tris(2-carboxyethyl)phosphine; TIM, translocase of the inner membrane.

* Corresponding author at: Institute of Parasitology, Biology Center, Czech Academy of Sciences, 37005 České Budějovice, Czech Republic.
E-mail address: hassan@paru.cas.cz (H. Hashimi).

https://doi.org/10.1016/j.molbiopara.2022.111463
Received 2 November 2021; Received in revised form 7 January 2022; Accepted 9 February 2022
Available online 11 February 2022

intermolecular bridge between Mia40′s CPC motif and the substrate can be formed. During subsequent steps the substrate is oxidatively folded and released [9,10]. The folded IMS protein now cannot pass outer membrane pores and therefore becomes trapped in the IMS. Reduced Mia40 is reoxidized by the other core protein of MIA pathway, sulfhydryl oxidase Erv1 [11]. Electrons are further transferred from Erv1 to cytochrome *c* [12]. This system introducing disulfide bonds and shuttling electrons is named a disulfide relay. An analogous pathway exists in alphaproteobacteria such as *Escherichia coli*, in which protein oxidative folding in the bacterial periplasm is performed by the oxidoreductase DsbA [13]. In contrast to Mia40, DsbA belongs to the thioredoxin family of oxidoreductases.

Respiring mitochondria produce different reactive oxygen species (ROS) [14]. They can have a signalling function in the cell, but can also be toxic metabolites capable of oxidation of proteins and peroxidation of lipids, threatening cell viability. Thus intracellular ROS have to be carefully controlled by protective systems, the thioredoxin and glutathione redox buffer systems [15,16]. In the latter, the intracellular redox state is defined as the ratio of reduced glutathione (GSH) and oxidized glutathione disulfide (GSSG). GSSG is reduced by glutathione reductase. The proofreading activity of glutathione in the MIA disulfide relay was shown [12]. Thus, disulfide relay and the maintenance of the redox homeostasis in the IMS are tightly connected [17].

Mia40 has a spotty distribution in eukaryotes, being found in the Opsithokonta (a supergroup containing animals and fungi), amoebozoans and land plants and jakobid protists [18–20]. It is conspicuously absent from trypanosomatids and related euglenozoans, even though its genome encodes twin C(X3)C and C(X9)C motif proteins with high-confidence ITSs [5,21]. In contrast, Erv1 is found in virtually all aerobic eukaryotes, including trypanosomatids [18,22]. Indeed, characterization of Erv1 from *Trypanosoma brucei* [14] and *Leishmania tarentoloe* [15] demonstrated that they have oxidoreductase activity and reduce cytochrome *c*. Also, RNAi-mediated depletion of *T. brucei* Erv1 leads to downregulation of twin C(X3)C or C(X9)C motif-bearing proteins that undergo oxidative folding in the IMS [24]. Further evidence of trypanosomal Erv1′s conserved function is that a single cysteine replacement in *L. tarentolae* Erv1 (LtErv1) renders the oxidoreductase adequately compatible with the yeast MIA pathway, as demonstrated by its capacity to complement the Δ*erv1* mutant in baker's yeast [25]. Thus, while Erv1 has been established as the final oxidoreductase in MIA disulfide relay, the presence of an enzyme that initiates oxidative folding of twin C(X3)C or C(X9)C motif-bearing IMS proteins remains mysterious.

The lack of a Mia40 homolog is consistent with the mitochondrial protein import machinery of trypanosomatids having many highly divergent properties relative to those of well-studied opisthokont model organisms [26]. Another factor that may contribute to the divergence of the MIA pathway is that trypanosomatids utilize trypanothione instead of glutathione as its redox buffering system [27–29]. Trypanothione is a kinetically-favoured dithiol reductant, making it much more reactive than glutathione. Thus, it is possible that this unique redox buffering system may have led to adaptations in the MIA system, such as a Mia40-replacement.

The trypanosomal MICOS complex is involved in the morphogenesis of cristae, the hallmark invaginations of the mitochondrial inner membrane, a conserved function common to opisthokont MICOS [30–32]. Unlike laterally organized yeast MICOS, trypanosomal MICOS consists of integral, membrane-anchored and peripheral, intermembrane space localized subcomplexes [30]. Unexpectedly, trypanosomal MICOS appears to be involved in the import of twin C(X3)C or C(X9)C motif-bearing IMS proteins [31]. This observation may be correlated with MICOS containing a subunit with a thioredoxin-fold and a potentially catalytic CIPC motif [33]. We hypothesized that this subunit, named TbMic20, may have replaced Mia40 in trypanosomatids by catalysing the oxidative folding of twin C(X3)C or C(X9)C motif-bearing proteins in the IMS. Here, we set about validating or refuting this hypothesis.

2. Results

2.1. TbMic20 depletion affects the abundance of IMS proteins but does not affect TbErv1 dimerization or redox state

We used previously established procyclic *T. brucei* TbMic20 doxycycline (Dox)-inducible RNAi cell line [31]. Proteins obtained from this cell line were resolved by SDS PAGE gel and subsequently subjected to immunoblotting with antibodies recognizing various mitochondrial proteins (Fig. 1 A). This analysis reveals high efficiency of RNAi: 2 days after RNAi-induction TbMic20 was already undetectable. A certain degree of depletion in TbTim9 and TbErv1, representative IMS proteins becomes prominent on day 4 after TbMic20 silencing. A noticeable depletion of the matrix-targeted protein TbCoxIV, and simultaneous accumulation of its unprocessed form retaining its pre-sequence, appears on day 6, and is a secondary effect on protein import [30]. Matrix protein TbHSP70 was not significantly affected. Enolase, a cytosolic protein, was used as a loading control. The results here are consistent with prior results indicating the TbMic20 and other subunits of the peripheral MICOS subcomplex play a role in IMS protein import and/or processing [30,31].

The working hypothesis at the beginning of our study was that TbMic20 is functionally analogous to opisthokont Mia40. If so, TbMic20 depletion may influence the redox state of TbErv1, that normally exists as a covalent dimer in yeast and *Leishmania tarentolae* [23,34]. Probing with polyclonal antibodies recognizing TbErv1 revealed a band of double the TbErv1 molecular weight that disappeared when treated with reducing agent tris(2-carboxyethyl)phosphine (TCEP) (Fig. 1B), thus verifying it is indeed the TbErv1 dimer. Analyzing samples of intact cells and TbMic20 depleted cells, we found that, though the abundance of TbErv1 is decreased after 3 days of TbMic20 depletion, the apparent ratio of TbErv1 dimers to monomers remains the same. The stability of TbErv1 dimers indicates that TbMic20 is not responsible for dimerization of TbErv1.

Furthermore, we addressed whether TbMic20 depletion affects the redox state of TbErv1, since the enzyme has 3 dicysteine motifs that are engaged in several inter- and intramolecular disulfides [22,23]. For that purpose, cells were treated with N-ethylmaleimide (NEM), which attaches to free thiols and prevents their reshuffling. Cells not treated by NEM were subjected to a thiol trapping assay, in which proteins immediately precipitated with trichloroacetic acid (TCA) were incubated with 4-acetamido-4-maleimidylstilbene-2,2-disulfonic acid (AMS), a compound that attaches to free thiols and increases molecular weight of the protein by 0.5 kDa per moiety. Already existing disulfide bonds remain intact and thus their constituent cysteines are not labelled with AMS. Samples preliminarily reduced with DL-Dithiothreitol (DTT) were also treated with AMS to show how a fully reduced TbErv1 appears in this assay (Fig. 1 C). All these variations from TbMic20 RNAi cell lines grown for three days in presence and absence of Dox were resolved by SDS PAGE (Fig. 1D). TbErv1 from AMS-treated samples (lanes 3 and 4 in Fig. 1D) appear slightly larger than from the NEM-treated cells (lanes 1 and 2). Given that NEM does not add enough mass to proteins to shift their SDS PAGE mobility, we interpret this to mean that the AMS likely binds to a thiol present on a single cysteine near the N-terminus of Erv1 from trypanosomatids [25], indicating the AMS trapping assay works. Samples were also pre-treated with DTT prior to AMS-conjugation to reveal how fully reduced TbErv1 appears in this assay (lanes 5 and 6). TbErv1 has seven cysteine residues. Therefore, the fully reduced form after treatment with DTT is expected to have 7 AMS molecules attached to each TbErv1 monomer, which would increase its size by 3.5 kDa. The shift of the band in fully reduced samples (lanes 5 and 6) in relation to samples untreated with IMS (lanes 1 and 2) corresponds to the expected value. However, the lack of any differences in TbErv1 between TbMic20-depleted samples and untreated controls excluding DTT

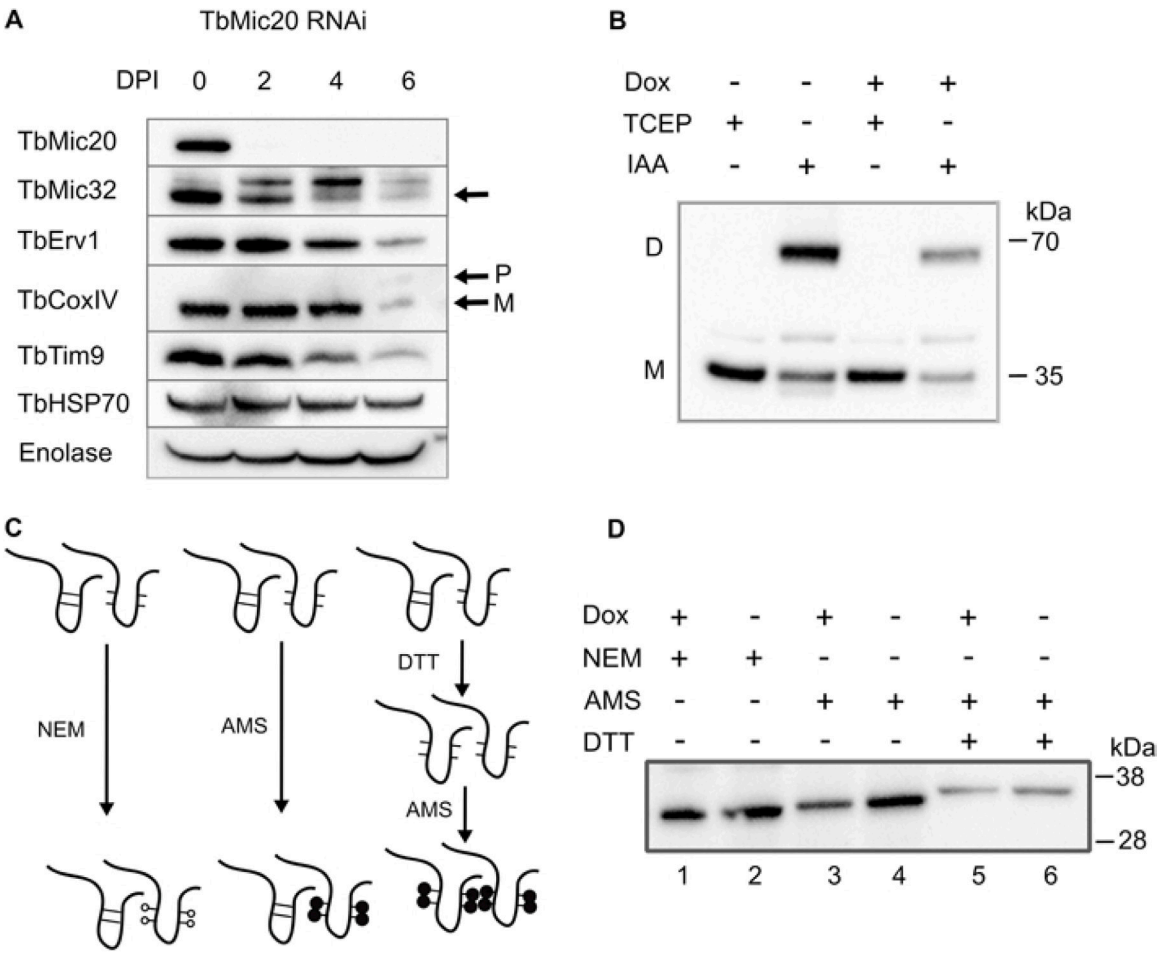

Fig. 1. **(A)** Effects of TbMic20 RNAi depletion on the abundance of selected mitochondrial proteins (indicated on left) over a 6-day time course (top). Arrow indicates specific TbMic32 band; P, precursor TbCoxIV form, M, mature TbCoxIV after cleavage of presequence. **(B)** TbErv1 dimerization and the effect of TbMic20 depletion on dimers. TbMic20 RNAi cell line was induced during three days. A representative image from 3 replicates of a polyclonal anti-TbErv1 antibody signal is shown here. D, dimer; M, monomer. **(C)** Schematic representation of the experiment to determine the redox state of the protein. Free thiols are blocked with NEM to prevent their reshuffling; disulfide bonds are reduced with DTT; AMS adds 0.5 kDa to every free thiol, which retards protein migration through gel during SDS-PAGE. **(D)** Redox state of Erv1 in TbMic20 RNAi -induced and non-induced cells. The band corresponding to the monomer is shown. Lanes are numbered below. DPI, days post induction; Dox, doxycycline; NEM, N-ethylmaleimide; TCEP, tris(2-carboxyethyl)phosphine; IAA, Iodoacetamide.

treatment indicates that the redox state of TbErv1 is not influenced by TbMic20 (Fig. 1D, *c.f.* lanes 3 and 4).

2.2. Point mutations in TbMic20 CIPC motif affect cell viability and the abundance of IMS proteins

Next, we assessed the importance of the hypothesized catalytic CIPC motif of TbMic20, one feature that led to its annotation as a thioredoxin-like protein [31]. To this end, we transformed a cell line capable of Dox-inducible expression of long-hairpin RNA [35], which eventually depletes endogenous and HA-tagged Mic20 protein, with three constructs that facilitate Dox-inducible expression of recoded His-tagged Mic20 (Fig. 2A). Recoding of Mic20 ORFs within this construct allows for expression of a RNAi-refractory form of Mic20. One of three Mic20 forms were electroporated: WT, which bears the unchanged CIPC motif, C80A mutant that mutates the first cysteine at position 80 of the motif to alanine, and C83A that mutates the second active site cysteine.

The depletion of endogenous and HA-tagged TbMic20 and expression of recoded TbMic20 isoforms in all three cell lines upon Dox induction were verified by Western blot (Fig. 2B). Noticeable difference in the abundance of the expressed recoded proteins relative to WT was consistent through two attempts of establishing these cell lines, each resulting in 4–5 clones. However, it should be noted that while the mutant forms are less abundant than the recoded-WT, they are expressed at an equivalent to higher level than the endogenous and HA-tagged TbMic20 in the non-induced samples (Fig. 2B, *c.f.* lane 1 with lanes 3 and 4; also see Table 1). Western analysis demonstrated that the recoded-WT TbMic20 replenishes the levels of IMS proteins TbErv1 and TbTim9, plus the matrix-imported TbCOIV in RNAi cells during a 6-day time course (Fig. 2C); enolase was used as a loading control. This result confirms that recoded-WT Mic20 successfully complements RNAi-depletion of Mic20. To verify that expressed recoded TbMic20 isoforms are targeted to the mitochondrion, digitonin fractionation was performed after Dox-induction. All recoded TbMic20 isoforms were detected in crude mitochondria fraction and absent from cytosolic fraction, that indicates their successful import (Fig. 2D).

Growth rates of recoded cell lines and RNAi were followed for six days after induction and compared with the growth of non-induced cell lines. Expression of WT isoform combined with simultaneous RNAi depletion of endogenous TbMic20 did not affect cell growth (Fig. 2E), demonstrating this form complemented the depletion of RNA-silenced TbMic20. C80A expression under the same conditions slightly reduced the growth rate, and expression of C83A resulted in pronounced growth phenotype, comparable with that of TbMic20 RNAi cell line (Fig. 2E).

To further investigate the effect of cysteine mutations, we set out to determine the depletomes (*i.e.* inventory of downregulated proteins) of

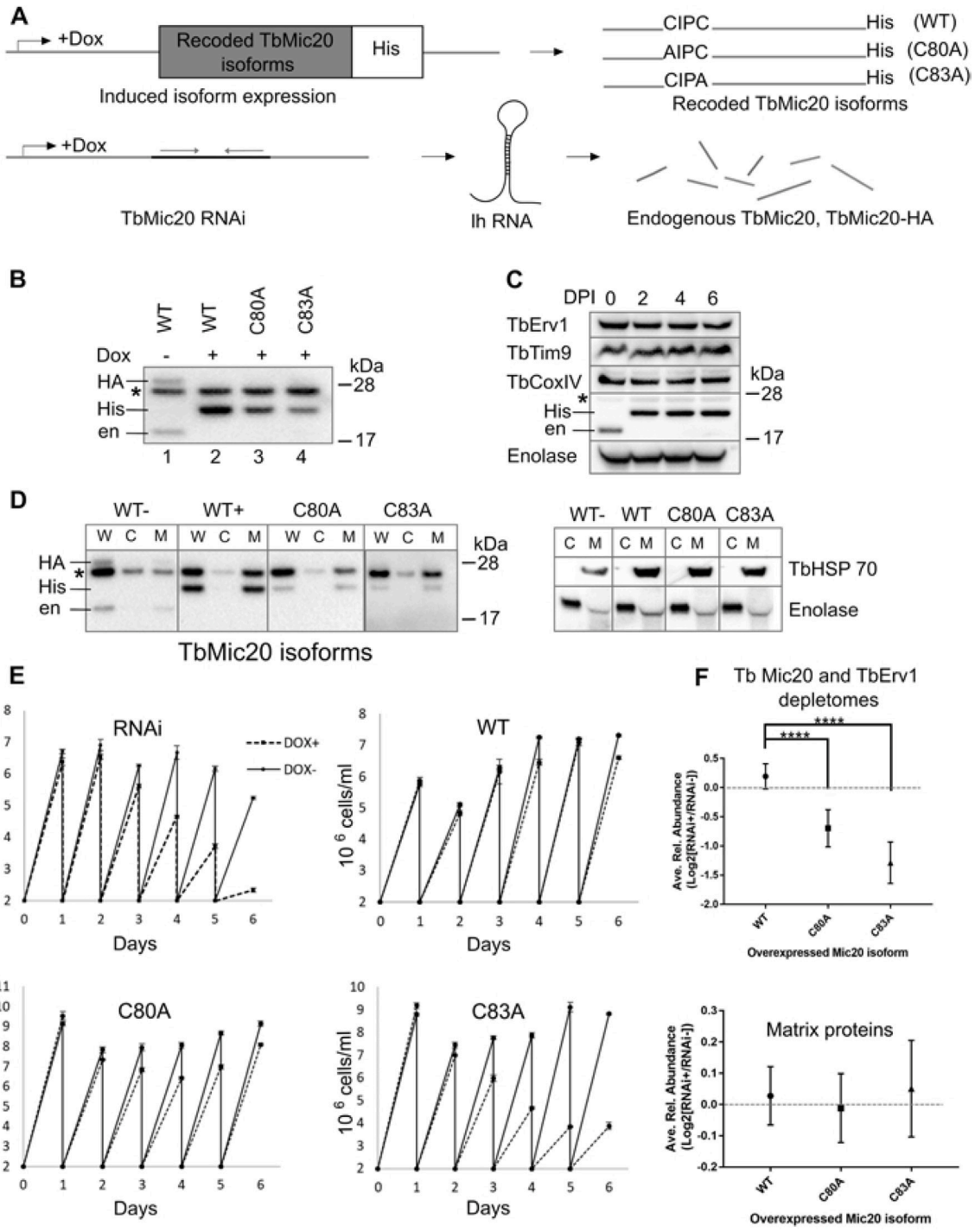

Fig. 2. Effects of recoded TbMic20 WT and CIPC mutants on proteins imported into the IMS *via* oxidative folding. **(A)** Simultaneous induced expression of His-tagged recoded TbMic20 isoforms and long hairpin RNAi (lhRNAi) targeting *TbMic20* mRNA for degradation upon doxycycline (Dox) induction, which leads to depletion of endogenous TbMic20. **(B)** comparison of recoded TbMic20 WT and CIPC mutants expression. HA, TbMic20 with C-terminal HA tag; en, endogenous TbMic20; His, overexpressed TbMic20 with C-terminal His and Myc tag; * , non-specific band, which also serves as a loading control. Lanes are numbered below. A representative image from five replicates is shown. **(C)** Effects of TbMic20 WT expression on the abundance of selected mitochondrial proteins (indicated on the left) over a 6-day time course (top). DPI, days post induction; other labels as in **B**. **(D)** Subcellular distribution of recoded Mic20 WT and CIPC mutants after 3 days of induction with doxycycline (Dox). W, whole cell lysate; C, cytosolic fraction; M, mitochondrial fraction; * , non-specific band. Right panel: subcellular fractionation verified with cytosolic and mitochondrial markers, enolase and HSP70, respectively. **(E)** Growth rates of Dox-induced cells expressing indicated TbMic20 isoforms and of TMic20 RNAi compared to non-induced cells. Data points plot the mean of biological triplicates with error bars indicating standard deviation. **(F)**: The relative abundance of proteins affected in the combined TbMic20 and TbErv1 depletomes according to [24], [31] (upper panel). The abundance of matrix proteins was used as a control (panel below). Dashed line highlights the absence of changes in relative protein abundance. Related to Dataset S1.

Table 1
Relative expression levels of recoded TbMic20 isoforms compared to endogenous TbMic20. Related to Dataset 1.

	Relative abundance Log_2 (Dox+/Dox-)[a]		
TbMic20 isoform	Replicate 1	Replicate 2	Ave.±SD[b]
WT	1.84	2.39	2.11 ± 0.28
C80A	3.19	3.54	3.37 ± 0.18
C83A	0.18	2.88	1.53 ± 1.35

[a] Log2 value equal to 0 means no difference in expression of TbMic20 in presence and absence of doxycycline (Dox) (*i.e.* recoded TbMic20 isoform expressed at same level endogenous TbMic20).
[b] SD, standard deviation.

each Dox-induced cell line compared to their downregulated counterparts as we had performed previously [31]. WT, C80A and C83A cell lines were Dox-induced in duplicates for 3 days. Subsequently, induced and non-induced cells were collected, fractionated by digitonin treatment and enriched mitochondrial fractions were submitted for mass spectrometry (LC-MS/MS) analysis. The relative abundancies of the proteins belonging to the TbMic20 [31] and TbErv1 [24] depletomes were reduced in C80A and C83A cell lines in comparison with WT (Fig. 2F), thus phenocopying TbMic20 RNAi with high statistical significance. To be sure that the observed changes in IMS protein abundancies are specific, we also addressed the abundance of matrix proteins as defined in our previous study [31]. Expression of any isoform did not significantly affect the abundance of this group (Fig. 2F). Thus, cysteine mutations in the CIPC motif of TbMic20 specifically affect the import and/or processing of IMS proteins without interference of protein import to other mitochondrial compartments 3 days after Dox-induction. We therefore conclude that the TbMic20 CIPC motif cysteines are essential for the apparent involvement of the trypanosomal MICOS complex in IMS import.

2.3. Recombinant TbMic20 exhibits a redox potential similar to other thioredoxins and oxidoreductases

Recombinant TbMic20 (rTbMic20) with a C-terminal His-tag was expressed in *Escherichia coli* and affinity purified. The His-tag was cleaved from the eluted protein with AcTEV protease, which is visible when the products of this reaction are resolved by SDS-PAGE and stained with Coomassie Brilliant Blue (Fig. 3A). The resulting recombinant protein was then used to determine TbMic20′s midpoint voltage following as established pipeline used for Mia40 [8] and other thioredoxin-like proteins [36,37]. Prior to redox potential measurement an emission scan at 280 nm excitation wavelength was performed to determine the wavelength with maximal difference in fluorescence intensity for fully reduced and oxidized TbMic20, which was determined to be 333 nm (Fig. 3B). Next, we determined the redox equilibrium of rTbMic20 at different ratios of GSH and GSSG by measuring the fluorescence intensity of emitted 333 nm light, which allowed us to infer the fraction of reduced protein [8,36,37]. The equilibrium constant (K_{eq}) of TbMic20 was estimated by linear transformation of the data in Fig. 3C as described in Materials and Methods. This K_{eq} allowed us to ultimately estimate the standard redox potential of rTbMic20, − 187,97 mV (Fig. 3D), which is in the range of midpoint voltage for other thioredoxin-like proteins, such as ScErv1, PDI, ScMia40 (Fig. 3E). Thus, we conclude that redox potential of TbMic20 indeed is close to Mia40 and other thioredoxin-like proteins.

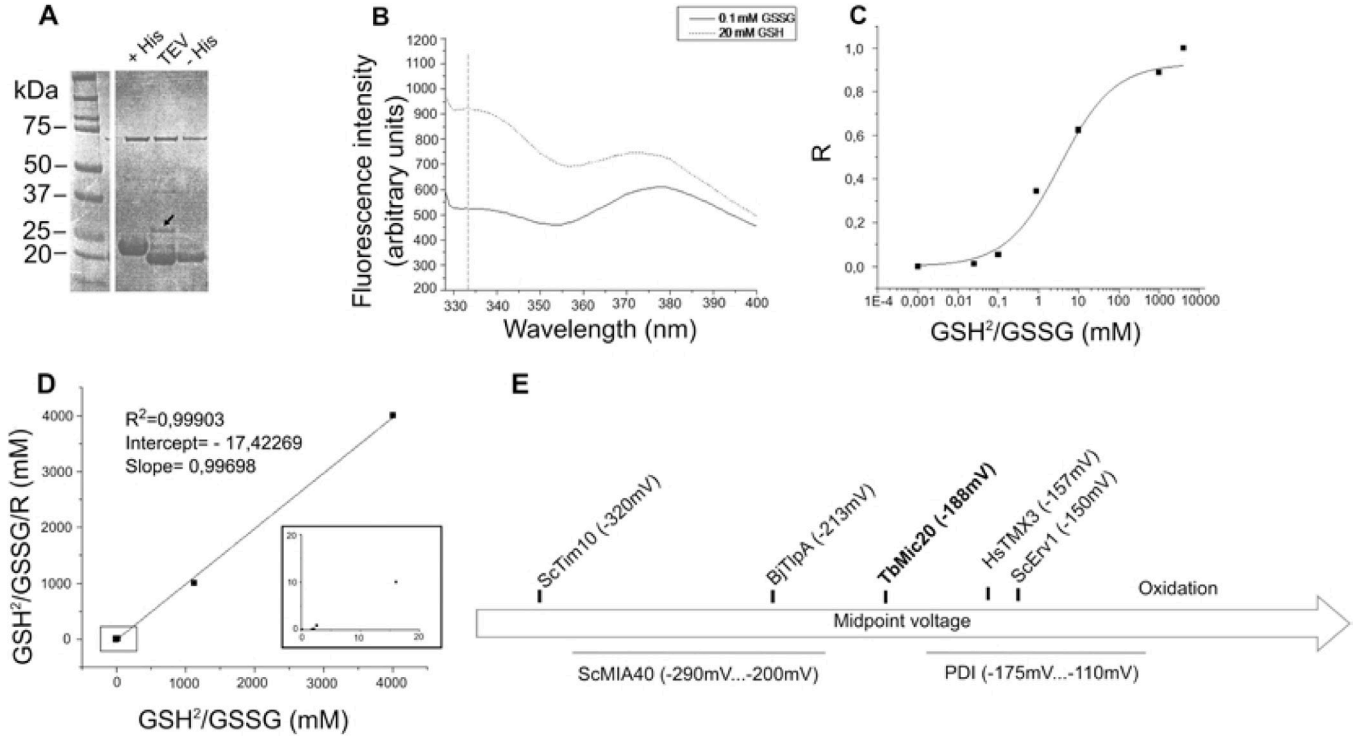

Fig. 3. The estimated redox potential of TbMic20 is similar to other thioredoxins and oxidoreductases. **(A)**: Purification and cleavage of recombinant His-TbMic20. + His, affinity purified recombinant TbMic20, with C-terminal His tag; TEV, TbMic20 with His-tag cleaved; -His, affinity purified TbMic20. Arrow indicates the band of AcTEV protease (27 kDa). **(B)**: Emission spectra of reduced and oxidized TbMic20 after excitation at 280 nm. Maximum difference in the fluorescence intensity (333 nm) is indicated with dashed line. **(C)**: The redox equilibrium of rTbMic20 at different ratios of $[GSH]^2/[GSSG]$. **(D)**: Estimation of the redox equilibrium K_{eq} by linear transformation of data in C. Inset shows data points from lower GSH concentrations not visible in the main graph that was used for trendline fitting. R^2, slope and y-intercept of trendline shown in large graph. **(E)**: comparison of TbMic20 redox potential with that of several IMS/periplasm proteins: ScTim10 [60], human thioredoxin-related transmembrane protein 3 (HsTMX3) [37], PDI [58], Mia40 [8], [61], ScErv1 [61], bacterial thioredoxin-like protein (BjTlpA) [36].

2.4. The CIPC motif of TbMic20 is reduced in vivo

After determining redox potential of recombinant TbMic20, we next addressed what is the redox state of the CIPC motif *in vivo*. According to the model of opisthokont MIA pathway, cysteines of the CPC motif in Mia40 are oxidized at steady state, *i.e.* they form a intramolecular disulfide bridge, in order to be able to accept electrons from reduced substrate proteins to facilitate their oxidative folding and ultimate retention in the IMS [2,3]. Hypothesizing about functional analogy between Mia40 and TbMic20, we decided to address the redox state of TbMic20 *in vivo*. Against our expectations, the experiment revealed the presence of reduced thiols in TbMic20 (Fig. 4 A), forcing us to reject the hypothesis that TbMic20 can be a Mia40 replacement.

In addressing the function of TbMic20, we attempted to complement *Escherichia coli dsbA* deletion mutants with TbMic20. This gene encodes DsbA, a thioredoxin that is the main catalyst of oxidative folding of proteins in the periplasm [38]. To test the hypothesis that TbMic20 can perform oxidative folding in the periplasm, we expressed TbMic20 appended with the 11 amino acid N-terminal periplasm-targeting sequence of DsbA in Δ*dsbA E. coli*. One of DsbA substrates is the flagellar P-ring component FlgI [39], which is not properly folded in Δ*dsbA E. coli*, thus having impaired flagellar assembly and a consequent lack of motility. The difference between wild type and Δ*dsbA* cells is easily detected when bacteria are seeded on semisolid agar plates. When a drop of bacterial culture is put in the center of the plate, motile bacteria spread all over the plate after overnight incubation. Non-motile cells stay in the center. The expression of DsbA or another protein capable of oxidative folding of FlgI in Δ*dsbA* cells restores the motility (Fig. 4B). rTbMic20, expressed in Δ*dsbA E. coli* cells, did not restore cell motility (Fig. 4 C). Hence, in *E. coli* TbMic20 is not able to perform oxidative folding, at least under the experimental conditions used here.

3. Discussion

MIA substrates enter the IMS in reduced state, where they undergo oxidative folding for their maturation and retention in this compartment [3]. The central MIA oxidoreductase introduces disulfide bonds into the MIA substrate for this purpose. Such an enzyme needs to have its active site dicysteines oxidized, *i.e.* linked by a disulfide bridge, to accept electrons from the reduced thiols present on the freshly imported MIA substrate. This is indeed observed on the CPC motif of Mia40 [40]. In the periplasm of bacteria, which is analogous to the IMS, oxidoreductases are also present and the oxidative folding pathway analogous to MIA exists [41]. The active CPHC motif of the central catalyst DsbA, the bacterial oxidoreductase analogous to Mia40 [13], is also oxidized [42]. Thus, we would expect the same for any functional analog of Mia40. Nevertheless, our study demonstrated that TbMic20 is reduced *in vivo*. That goes against our initial hypothesis and casts doubt on functional analogy between Mia40 and TbMic20. Also, there is no obvious motif on TbMic20 for recognizing the ITS of MIA substrates, which is a hydrophobic cleft formed by two α-helices joined by twin disulfide bridges [6,8], also arguing against TbMic20 completely replacing Mia40. In addition, TbMic20 could not complement DsbA function in *E. coli*. However, it should be noted that the failure of TbMic20 to complement Δ*dsbA* may be due to its failure to recognize periplasmic substrates instead of the reduced state of its CIPC motif.

On the other hand, cysteine mutations in CIPC motif of TbMic20 result in significant reduction of IMS proteins and phenocopy depletion effect of TbMic20 and TbErv1 RNAi. Thus, TbMic20 and its CIPC motif in particular appears to play significant, but still undefined role in IMS protein import and/or processing. We should note that although cysteine to alanine mutations we employed here have been used previously in the functional analysis of thioredoxins [43], we acknowledge that this conversion to a non-polar amino acid may have affected protein folding in addition to disrupting the disulfide bridge of the motif. Indeed, the lower expression of the mutants in comparison with the recoded-WT TbMic20 may be a consequence of this. However, we favor the interpretation that the observed lower expression of the mutants is due to a downstream effect on IMS protein import observed in these mutants. Indeed, we show that the mutant forms of TbMic20 are successfully imported into the mitochondrion and exhibit steady-state levels equivalent to endogenous and *in situ* tagged TbMic20. Given that IMS import defects due to TbErv1 also affects TbMic20 levels [24], it is possible that the cysteine mutants may impact Mic20 in a similar

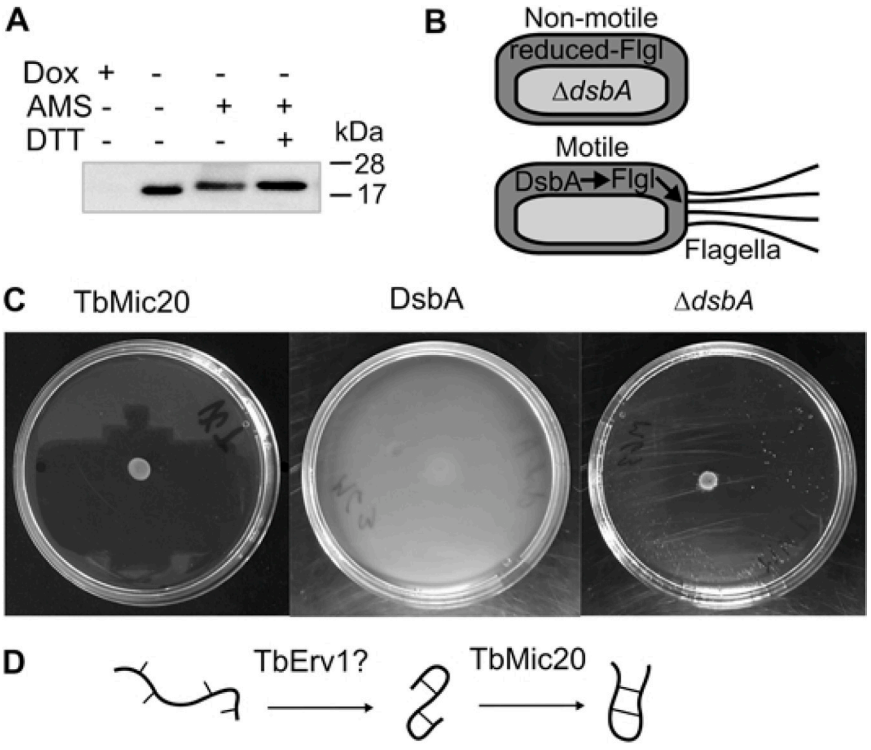

Fig. 4. (A): Redox state of TbMic20 *in vivo,* with cells undergoing 3 days of *TbMic20* RNAi to show band specificity. A representative image from 4 replicates is shown here. Dox, doxycycline; AMS, 4-acetamido-4-maleimidylstilbene-2,2-disulfonic acid; DTT, DL-Dithiothreitol. **(B)**: Schematic representation of DsbA deletion effect on cell motility: Δ*dsbA* mutant is non-motile because FlgI protein oxidative folding is impaired, resulting in improper flagellar assembly and loss of motility. **(C)**: Swarming motility in *E. coli* expressing TbMic20 and DsbA in the Δ*dsbA* mutant in comparison with Δ*dsbA* mutant alone. **(D)**: Hypothetical role to TbMic20 as an isomerase in case TbErv1 is the central catalyst of MIA pathway in trypanosomatids.

way. Nevertheless, our results show that each cysteine in CIPC motif is important for TbMic20.

Taking into consideration both the fact that TbMic20 is most likely not the central catalyst of the MIA pathway, but nevertheless appears to be involved to some extent in IMS import *via* its CIPC motif, we now offer alternate hypotheses on what possible roles it can play in this process. One is that TbMic20 acts as an isomerase, reshaping mispaired disulfide isomers of IMS substrates (Fig. 4D). This function is similar to that of the protein disulfide isomerase (PDI), a multifunctional protein localized in the lumen of endoplasmic reticulum [44,45]. One of the main PDI functions is rearranging disulfide bonds in misfolded protein substrates [46]. In *T.brucei*, such an isomerase activity may be essential in the case that TbErv1 directly oxidizes MIA substrates, as has been proposed in *Arabidopsis thaliana* [47]. In this scenario, we propose that direct oxidative folding by TbErv1 may result in aberrant folding of MIA substrates, which are ultimately repaired by a putative chaperone activity of TbMic20 (Fig. 4D). Alternatively, such misfolding may be more predominant in the presence of trypanothione, which is a kinetically faster dithiol reductant than the more universal glutathione redox buffer that is present in Mia40 containing eukaryotes [19,27,28].

Another possibility is that TbMic20 has auxiliary role in the IMS such as maintaining the redox state of yet unidentified functional analog of Mia40. Some examples of such proteins are known from other model organisms. For instance, in *S. cerevisiae* thiol peroxidase Gpx3, localized in the IMS, promotes Mia40 dependent protein folding [48]. Candidates for the Mia40 replacement in kinetoplastids were recently identified in the TbErv1 interactome of a related trypanosomatid species, *Leishmania tarentolae* [49].

In conclusion, we have demonstrated that the CIPC motif of TbMic20 is necessary for a still unidentified role in IMS import in trypanosomatids. While our study was performed in procyclic stage *T. brucei*, a high-throughput RNAi-screen of *T. brucei* proteins suggests that TbMic20 is essential in the bloodstream stage as well [50], implying its importance in the biogenesis of mitochondria that exhibit both reduced cristae and role in energy metabolism [51,52]. Nevertheless, direct oxidative folding by TbMic20 is highly unlikely due to the reduced state of the enzyme *in vivo*. Thus, we offer alternate hypotheses to explain why TbMic20 depletion and mutation impacts the levels of IMS proteins bearing twin C(X3)C or C(X9)C motifs. In one, we speculate that the oxidoreductase activity of TbMic20 facilitates the isomerization of misfolded MIA substrate proteins (Fig. 4D). The other is that TbMic20 has an auxiliary function in maintaining the activity of a putative Mia40 replacement in trypanosomatids. However, while the results presented here force us to question our initial hypothesis that TbMic20 is a *bona fide* Mia40 replacement, the effect of TbMic20 depletion or mutation on the levels of proteins imported into the IMS *via* the MIA pathway allows us to maintain our original notion: trypanosomal MICOS is involved in the maturation and/or stability of these proteins [30–32].

4. Materials and methods

4.1. TbMic20 mutant cell lines

Procyclic *T. brucei* cultivation, generation of transgenic cell lines, and growth measurements were performed as previously described [31]. TbMic20 open reading frames (ORFs), partly recoded and containing mutations were commercially synthetized by General Biosystems (USA) and cloned into pcDNA3.1(+) myc-His A vector. The sequences of the isoforms are listed below. Each isoform was PCR-amplified and cloned in pT7–3xV5 destination vector [53]. They were used to transfect a previously obtained *T. brucei* cell line with TbMic20 C-terminally HA-tagged and incorporated inducible TbMic20 RNAi construct [31].

TbMic20 isoforms. Recoded part is underlined, the codon where cysteine is substituted to alanine, is in bold and lowercase.

TbMic20-RNAi refactory (WT):

GGTACCATGGGTTCTCATCATCATCATCATCATGGTTCTGG-
TAGTGGTTCCGGTTCCGGTTCTAAGCTTATGACCCAAAACATTATTCGT
CGCATCTTTGGCAATCGTGAACTGCCGGAGAACCTTAGTGGTAGCGA
GTATGAGCGCTATATGCAGGAAAATTTTCCCAAATGGATTGA
TGAATTTGAAAAGGGTGGGTTTCTTGAAGCAACAAAACTTCCAGCCA-
TAAAAAGTGAGAGGGACTTCTTGAGCAAGCTCATTGAACATAAA-
GACGAAATCATGGTGGTTAAATACTGGAAGCATGGATGCATCCCAT
GCCTCTCACTTGCGGAAATGTATAAACAGGTATCAGAGCAATGCAA-
GAAAGAAAACCGTCGTATTGCATGGTACAGTGTTAATACAAAAGAC
GTTAGCGCGCGTTCGTTAGTTGATTACCAACTCGTGAACGGAACCC-
CAACAGTCCAGACGTTCAGTCGTATGAAACAGGTTGGTAAAGAAAT
CCGAGCAATAAGCGCGGAGGAGCTTATGAGGGAGCTTTCTTTA
CGCGAGGCTGCTCTGAATACAGAGAGTTCTAGA.

C80AMutant-RNAi refactory:

GGTACCATGGGTTCTCATCATCATCATCATCATGGTTCTGGTAGT
GGTTCCGGTTCCGGTTCTAAGCTTATGACCCAAAACATTATTCG
TCGCATCTTTGGCAATCGTGAACTGCCGGAGAACCTTAGTGGTAGCG
AGTATGAGCGCTATATGCAGGAAAATTTTCCCAAATGGATTGATGAAT
TTGAAAAGGGTGGGTTTCTTGAAGCAACAAAACTTCCAGCCATAAAA
AGTGAGAGGGACTTCTTGAGCAAGCTCATTGAACATAAAGACGAA
ATCATGGTGGTTAAATACTGGAAGCATGGA**gca**ATCCCATGCCTCTCAC
TTGCGGAAATGTATAAACAGGTATCAGAGCAATGCAAGAAAGAAAA
CCGTCGTATTGCATGGTACAGTGTTAATACAAAAGACGTTAGCGC
GCGTTCGTTAGTTGATTACCAACTCGTGAACGGAACCCCAACAGTCCA-
GACGTTCAGTCGTATGAAACAGGTTGGTAAAGAAATCCGAGCAA-
TAAGCGCGGAGGAGCTTATGAGGGAGCTTTCTTTACGCGAGGCTGC
TCTGAATACAGAGAGTTCTAGA.

C83AMutant-RNAi refactory:

GGTACCATGGGTTCTCATCATCATCATCATCATGGTTCTGGTAGT
GGTTCCGGTTCCGGTTCTAAGCTTATGACCCAAAACATTATTCGTCG
CATCTTTGGCAATCGTGAACTGCCGGAGAACCTTAGTGGTAGCGAGTA
TGAGCGCTATATGCAGGAAAATTTTCCCAAATGGATTGATGAAT
TTGAAAAGGGTGGGTTTCTTGAAGCAACAAAACTTCCAGCCATAAAAA
GTGAGAGGGACTTCTTGAGCAAGCTCATTGAACATAAAGACGAAATC
ATGGTGGTTAAATACTGGAAGCATGGATGCATCCCA**gca**CTCTCAC
TTGCGGAAATGTATAAACAGGTATCAGAGCAATGCAAGAAAGAAAAC
CGTCGTATTGCATGGTACAGTGTTAATACAAAAGACGTTAGCGCGC
GTTCGTTAGTTGATTACCAACTCGTGAACGGAACCCCAACAGTCCA-
GACGTTCAGTCGTATGAAACAGGTTGGTAAAGAAATCCGAGCAA-
TAAGCGCGGAGGAGCTTATGAGGGAGCTTTCTTTACGCGAGGCTGC
TCTGAATACAGAGAGTTCTAGA.

Primers for isoform PCR amplification. Lower case indicates the part of the sequence complementary to pT7–3X-V5 destination vector this construct will be cloned into by Gibson assembly [54].

F: ccaaaaagtaaaattcacaagctcctaggaagcttATGACCCAAAACATTATTC
GTCG.

R: taccttcgaaccgcgggccctctagggatccTCAATGGTGATGGTGATGATG
AC.

4.2. Samples preparation for LC-MS analyses

Crude mitochondria were prepared by digitonin fractionation on Dox-induced TbMic20 cell lines and non-induced negative controls as previously described [31]. Individual protein solutions were processed by filter-aided sample preparation (FASP) method [55] with some modifications. The samples were mixed with 8 M UA buffer (8 M urea in 100 mM Tris-HCl, pH 8.5), loaded onto the Microcon device with MWCO 30 kDa (Merck Millipore) and centrifuged at 7,000g for 30 min at 20 °C. The retained proteins were washed (all centrifugation steps after sample loading done at 14,000g) with 200 μL UA buffer. The final protein concentrates kept in the Microcon device were mixed with 100 μL of UA buffer containing 50 mM iodoacetamide and incubated in the dark for 20 min. After the next centrifugation step, the samples were washed three times with 100 μL UA buffer and three times with 100 μL of 50 mM NaHCO3. Trypsin (1 μg, sequencing grade, Promega) was added onto the filter and the mixture was incubated for 18 h at 37 °C.

The tryptic peptides were finally eluted by centrifugation followed by two additional elutions with 50 µL of 50 mM NaHCO3. Peptides were then cleaned by liquid-liquid extraction (3 iterations) using water saturated ethyl acetate [56]. Peptides were further transferred into LC-MS vials using 50 µL of 2.5% FA in 50% ACN and 100 µL of pure ACN and with addition of polyethylene glycol (final concentration 0.001%) and concentrated in a SpeedVac concentrator.

4.3. LC-MS analysis of peptides

LC-MS/MS analyses of all peptide mixtures were done using RSLCnano system connected to Orbitrap Fusion Lumos mass spectrometer (Thermo Fisher Scientific). Prior to LC separation, tryptic digests were online concentrated and desalted using trapping column (100 µm × 30 mm, column compartment temperature of 40ºC) filled with 3.5-µm X-Bridge BEH 130 C18 sorbent (Waters). After washing of trapping column with 0.1% FA, the peptides were eluted (flow rate - 300 nl/min) from the trapping column onto an analytical column (Acclaim Pepmap100C18, 3 µm particles, 75 µm × 500 mm; column compartment temperature of 40ºC, Thermo Fisher Scientific) by using 50 or 100 min long nonlinear gradient program (1–56% of mobile phase B; mobile phase A: 0.1% FA in water; mobile phase B: 0.1% FA in 80% ACN) for analysis of phosphopeptides enriched fraction or not enriched peptide mixture, respectively. Equilibration of the trapping column and the analytical column was done prior to sample injection to sample loop. The analytical column outlet was directly connected to the Digital PicoView 550 (New Objective) ion source with sheath gas option and SilicaTip emitter (New Objective; FS360–20–15-N-20-C12) utilization. ABIRD (Active Background Ion Reduction Device, ESI Source Solutions) was installed.

MS data were acquired in a data-dependent strategy selecting top 20 precursors based on the survey scan (350–2000 *m/z*). The resolution of the survey scan was 120,000 (200 *m/z*) with a target value of 4 × 105 ions and maximum injection time of 50 ms. HCD MS/MS (30% relative fragmentation energy, normal mass range) spectra were acquired with a target value of 5.0 × 104. The MS/MS spectra were recorded in Orbitrap at resolving power of 15 000 (200 *m/z*) and the maximum injection time for MS/MS was 22 ms. Dynamic exclusion was enabled for 60 s after one MS/MS spectra acquisition. The isolation window for MS/MS fragmentation was set to 1.2 *m/z*.

The analysis of the mass spectrometric RAW data files was carried out using the MaxQuant software (version 1.6.2.10) using default settings unless otherwise noted. MS/MS ion searches were done against modified cRAP database (based on http://www.thegpm.org/crap, 112 protein sequences) containing protein contaminants like keratin, trypsin *etc.*, and TriTrypDB protein database (http://tritrypdb.org/common/downloads/release-9.0/TbruceiTREU927/fasta/data/TriTrypDB-9.0_TbruceiTREU927_AnnotatedProteins.fasta; downloaded 8.12.2015, number of protein sequences: 11,567). Oxidation of methionine and proline, deamidation (N, Q) and acetylation (protein N-terminus) as optional modification, and trypsin/P enzyme with 2 allowed miss cleavages and minimal peptide length 6 amino acids were set. Peptides and proteins with FDR threshold < 0.01 and proteins having at least one unique or razor peptide were considered only. Match between runs was set for all sample replicates analyses. Protein intensities reported in proteinGroups.txt file (output of MaxQuant program) were further processed using the software container environment (https://github.com/OmicsWorkflows), version 3.7.1a. Processing workflow is available upon request. Briefly, it covered: a) removal of decoy hits and contaminant protein groups, b) protein group intensities log2 transformation, c) quantile normalization using limma R package and d) differential expression analysis (qualitative changes were considered using imputation on the sample minimum).

4.4. Redox state of TbMic20

Cells were lysed with SDS buffer containing reducing agent (50 mM DTT or 15 mM TCEP), 10 mM AMS or blocking agents, such as IAA (50 mM) or NEM (20 mM). The lysates were precipitated with trichloroacetic acid (TCA) solution in water to a final concentration 10% w/v on ice for one hour. Precipitated proteins were sedimentated for 15 min at 4 °C at 16,000 x g. Pellets were washed two times with 1 ml ice-cold acetone, dried on air and then resuspended with 1.5X SDS buffer. The DTT-treated samples were precipitated once again after treatment prior to AMS-conjugation. Four independent replicates were performed.

4.5. Expression and purification of rTbMic20

pSKB-3 plasmid [57], containing TbMic20 ORF and His-tag, was constructed and *Escherichia coli* BL21 strain transformed. To induce the expression of rTbMic20, Isopropyl-β-D-thiogalactopyranosid (IPTG) was added to a final concentration of 1 mM. Induction was performed at optical density at 600 nm (OD_{600}) of 0.6. Induced cells (200 ml) were incubated on a shaker at 200 RPM for 1 h at 37 C or overnight at 20 C. Cells were harvested for 10 min at 3000 g 4 C. The pellet was resuspended in 10 ml of lysis buffer, containing 50 mM NaH2PO4×2H2O, 300 mM NaCl and 10 mM of imidazole (pH 8.0) and sonicated with an ultrasonic homogenizer (BioLogic Inc. Ultrasonic Homogenizer Model 3000) six times for 10 s with 10 s pause at 50% power and 50% pulse. Homogenate was centrifuged as above to separate soluble fraction. rTbMic20 was purified utilizing BioRad Poly Prep Chromatography Column with 750 µL of Novex™ Ni-NTA Agarose (Invitrogen™) beads according to manufacturer's recommendations. Eluted fractions were analyzed on SDS-page gel. His tag was cleaved from rTbMic20 with AcTEV™ Protease (Invitrogen) following the manufacturer's instructions.

4.6. Determination of redox equilibrium

To determine the redox equilibrium between rTbMic20 and glutathione the former, purified and diluted to 5 µM in 50 µM degassed phosphate buffer (2X stock solution contains 20.701 g/l of Na_2H-PO_4•12 H_2O and 6.584 g/l of NaH_2PO_4 •2 H_2O; pH 7.0), was mixed with 0.1 mM GSSG and GSH in a range of concentrations from 0.01 mM to 20 mM. The mixtures in 500 µL aliquots were incubated for 16 h in an anaerobic chamber (Oxoid™ AnaeroJar™, ThermoFisher Scientific) and then loaded on a Nunc™ Micro Well™ 96-Well flat-bottom microplate. TECAN Spark® multimode-microplate-reader and the SparkControl application were used. After the wavelength with the maximal difference in fluorescence intensity of oxidized and reduced protein was determined (Fig. 3B), measurements were performed at following parameters: *Mode*: Fluorescence Intensity Scan Top Reading; *Excitation:* Monochromatic; *Excitation Wavelength*: 280 nm; *Excitation bandwidth*: 20 nm; *Emission wavelength*: 333 nm; *Gain:* 40; *Temperature*: 25 °C.

The redox equilibrium of TbMic20 with glutathione is given by Eq. (1). The relative amount of reduced TbMic20 (R) at equilibrium was calculated using Eq. (2) and plotted against the [GSH]2/[GSSG] ratio. The combination of Eqs. (2) and (3) to leads to Eq. (4). Linear transformation of this graph and fitting the data to Eq. (3), were used to determine the equilibrium constant K_{eq} [58]. The estimated K_{eq} was then used in the Nernst equation (Eq. 5), using the glutathione standard potential $E_{0(GSH/GSSG)}$ of − 0.240 V at pH 7.0 and 25 °C (ref 35), to estimate the midpoint voltage.

$$K_{eq} = \left[TbMic20^{S-S}\right] \quad [GSH]^2 \Big/ \left[TbMic20^{SH}\right] \quad [GSSG] \tag{1}$$

$$R = \left[TbMic20^{SH}\right] \quad \Big/ \left[TbMic20^{S-S}\right] + \left[TbMic20^{SH}\right] = (F - F_{ox})/(F_{red} - F_{ox}) \tag{2}$$

$$R = [GSH]^2/[\mathrm{GSSG}]/K_{eq} + [GSH]^2/[GSSG] \quad (3)$$

$$F = \frac{[\mathrm{GSH}]^2/[GSSG] \times (F_{red} - F_{ox})}{K_{eq} + [GSH]^2/[GSSG]} + F_{ox} \quad (4)$$

$$E_0 = E_{0(GSH/GSSG)} - \frac{RT}{nF} \times \ln(K_{eq}) \quad (5)$$

F…. measured fluorescence intensity
F_{red}…. Fluorescence intensity of reduced protein
F_{ox}……Fluorescence intensity of oxidized protein

4.7. Swarming motility assay

E. coli strains JFC207 (Δ*dsbA*) and JFC209 (*dsbA*$^+$) were obtained from the laboratory of Jean-François Collet at Institut de Duve, Université catholique de Louvain. Professor Collet also kindly provided pBad33::dsbA (PL81) vector bearing the *dsbA* ORF. This vector was also used for cloning the TbMic20 open reading frame downstream of the DsbA periplasm targeting sequence (the part encoding first 19 amino acids). The cells were maintained in LB medium supplied with 35 μg/ml chloramphenicol and, for JFC207, 50 μg/ml Kanamycin. TbMic20 ORF was amplified and cloned into pBad33 vectors by Gibson assembly [54]. *E. coli* cells were transformed with obtained constructs. The assay was performed as described before [59]: 100 μL of *E. coli* cell suspension, grown to OD_{600} of 0.4, were put in the centre of a semisolid agar plate and incubated overnight at 37 °C. Arabinose, which was present in the agar, induced plasmid expression.

Funding

This work was supported by Czech Science Foundation grant 20–23513S to H.H. and the Czech Ministry of Education grant OPVVV16_019/0000759. CIISB, Instruct-CZ Centre of Instruct-ERIC EU consortium, funded by MEYS CR infrastructure project LM2018127, is gratefully acknowledged for the financial support of the measurements at the CEITEC Proteomics Core Facility.

CRediT authorship contribution statement

Iosif Kaurov: Conceptualization, Investigation, Writing – original draft, Writing – review & editing, Visualization. **Jiří Heller:** Investigation. **Sebastian Deisenhammer:** Investigation. **David Potěšil:** Formal analysis, Investigation, Writing – original draft. **Zbyněk Zdráhal**: Writing – original draft; Supervision; Funding acquisition. **Hassan Hashimi:** Conceptualization, Formal analysis, Writing – original draft, Writing – review & editing, Visualization, Supervision; Funding acquisition.

Acknowledgments

We thank Julius Lukeš (Institute of Parasitology, University of South Bohemia) for his support. We also thank Jean-François Collet and Pauline Leverrier (Université catholique de Louvain) for *E. coli* strains, constructs and advice on swarming motility assay and André Schneider (University of Bern) for Tim9 antisera. We also thank Kostas Tokatlidis (University of Glasgow), Johnathan Beckwith (Harvard Medical School), Alan Fairlamb (University of Dundee) and Tamara Smutná (Charles University) for stimulating discussion.

Appendix A. Supporting information

Supplementary data associated with this article can be found in the online version at doi:10.1016/j.molbiopara.2022.111463.

References

[1] N. Wiedemann, N. Pfanner, Mitochondrial machineries for protein import and assembly, Annu. Rev. Biochem. 86 (1) (2017) 685–714.
[2] A. Mordas, K. Tokatlidis, The MIA pathway: a key regulator of mitochondrial oxidative protein folding and biogenesis, Acc. Chem. Res. 48 (8) (2015) 2191–2199.
[3] D. Stojanovski, P. Bragoszewski, A. Chacinska, The MIA pathway: a tight bond between protein transport and oxidative folding in mitochondria, Biochim. Biophys. Acta (BBA) - Mol. Cell Res. 1823 (7) (2012) 1142–1150.
[4] M. Deponte, K. Hell, Disulphide bond formation in the intermembrane space of mitochondria, J. Biochem. 146 (5) (2009) 599–608.
[5] I.E. Gentle, A.J. Perry, F.H. Alcock, V.A. Likic, P. Dolezal, E.T. Ng, A.W. Purcell, M. McConnville, T. Naderer, A.L. Chanez, F. Charriere, C. Aschinger, A. Schneider, K. Tokatlidis, T. Lithgow, Conserved motifs reveal details of ancestry and structure in the small TIM chaperones of the mitochondrial intermembrane space, Mol. Biol. Evol. 24 (5) (2007) 1149–1160.
[6] D.P. Sideris, N. Petrakis, N. Katrakili, D. Mikropoulou, A. Gallo, S. Ciofi-Baffoni, L. Banci, I. Bertini, K. Tokatlidis, A novel intermembrane space–targeting signal docks cysteines onto Mia40 during mitochondrial oxidative folding, J. Cell. Biol. 187 (7) (2009) 1007–1022.
[7] D. Milenkovic, T. Ramming, J.M. Müller, L.S. Wenz, N. Gebert, A. Schulze-Specking, D. Stojanovski, S. Rospert, A. Chacinska, Identification of the signal directing Tim9 and Tim10 into the intermembrane space of mitochondria, Mol. Biol. Cell 20 (2009) 10–2539.
[8] L. Banci, I. Bertini, C. Cefaro, S. Ciofi-Baffoni, A. Gallo, M. Martinelli, D.P. Sideris, N. Katrakili, K. Tokatlidis, MIA40 is an oxidoreductase that catalyzes oxidative protein folding in mitochondria, Nat. Struct. Mol. Biol. 16 (2) (2009) 198–206.
[9] L. Banci, I. Bertini, C. Cefaro, L. Cenacchi, S. Ciofi-Baffoni, I.C. Felli, A. Gallo, L. Gonnelli, E. Luchinat, D. Sideris, K. Tokatlidis, Molecular chaperone function of Mia40 triggers consecutive induced folding steps of the substrate in mitochondrial protein import, PNAS 107 (47) (2010) 20190–20195.
[10] M. Fischer, J. Riemer, The mitochondrial disulfide relay system: roles in oxidative protein folding and beyond, Int. J. Cell Biol. 2013 (2013) 1–12.
[11] N. Mesecke, N. Terziyska, C. Kozany, F. Baumann, W. Neupert, K. Hell, J. M. Herrmann, A disulfide relay system in the intermembrane space of mitochondria that mediates protein import, Cell 121 (7) (2005) 1059–1069.
[12] M. Bien, S. Longen, N. Wagener, I. Chwalla, J.M. Herrmann, J. Riemer, Mitochondrial disulfide bond formation is driven by intersubunit electron transfer in Erv1 and proofread by glutathione, Mol. Cell 37 (4) (2010) 516–528.
[13] J.C.A. Bardwell, K. McGovern, J. Beckwith, Identification of a protein required for disulfide bond formation in vivo, Cell 67 (3) (1991) 581–589.
[14] M. Schieber, N.S. Chandel, ROS function in redox signaling and oxidative stress, Curr. Biol. 24 (2014) R453–R462.
[15] F.Q. Schafer, G.R. Buettner, Redox environment of the cell as viewed through the redox state of the glutathione disulfide/glutathione couple, Free Rad. Biol. Med. 30 (11) (2001) 1191–1212.
[16] A. Holmgren, Thioredoxin and glutaredoxin systems, J. Biol. Chem. 264 (24) (1989) 13963–13966.
[17] J.M. Herrmann, R. Köhl, Catch me if you can! Oxidative protein trapping in the intermembrane space of mitochondria, J. Cell Biol. 176 (5) (2007) 559–563.
[18] J.W.A. Allen, S.J. Ferguson, M.L. Ginger, Distinctive biochemistry in the trypanosome mitochondrial intermembrane space suggests a model for stepwise evolution of the MIA pathway for import of cysteine-rich proteins, FEBS Lett. 582 (19) (2008) 2817–2825.
[19] S.A. Muñoz-Gómez, C.H. Slamovits, J.B. Dacks, J.G. Wideman, The evolution of MICOS: ancestral and derived functions and interactions, Com. Int. Biol. 8 (6) (2015), e1094593.
[20] C.W. Stairs, P. Táborský, E.D. Salomaki, M. Kolisko, T. Pánek, L. Eme, M. Hradilová, Č. Vlček, J. Jerlström-Hultqvist, A.J. Roger, I. Čepička, Anaeramoebae are a divergent lineage of eukaryotes that shed light on the transition from anaerobic mitochondria to hydrogenosomes, pp. 5605-5612.e5, Curr. Biol. 31 (24) (2021) 5605–5612.e5, pp. 5605-5612.e5.
[21] G. Cavallaro, Genome-wide analysis of eukaryotic twin CX9C proteins, Mol. BioSyst. 6 (12) (2010) 2459.
[22] S. Basu, J.C. Leonard, N. Desai, D.A. Mavridou, K.H. Tang, A.D. Goddard, M. L. Ginger, J. Lukeš, J.W. Allen, Divergence of Erv1-associated mitochondrial import and export pathways in trypanosomes and anaerobic protists, Euk. Cell 12 (2) (2013) 343–355.
[23] E. Eckers, C. Petrungaro, D. Gross, J. Riemer, K. Hell, M. Deponte, Divergent molecular evolution of the mitochondrial sulfhydryl:cytochrome *c* oxidoreductase Erv in opisthokonts and parasitic protists, J. Biol. Chem. 288 (4) (2013) 2676–2688.
[24] C.D. Peikert, J. Mani, M. Morgenstern, S. Käser, B. Knapp, C. Wenger, A. Harsman, S. Oeljeklaus, A. Schneider, B. Warscheid, Charting organellar importomes by quantitative mass spectrometry, Nat. Commun. 8 (1) (2017) 15272.
[25] S. Specht, L. Liedgens, M. Duarte, A. Stiegler, U. Wirth, M. Eberhardt, A. Tomás, K. Hell, M. Deponte, A single-cysteine mutant and chimeras of essential Leishmania Erv can complement the loss of Erv1 but not of Mia40 in yeast, Redox Biol. 15 (2018) 363–374.
[26] A. Schneider, Evolution of mitochondrial protein import – lessons from trypanosomes, Biol. Chem. 401 (6–7) (2020) 663–676.
[27] R.L. Krauth-Siegel, S.K. Meiering, H. Schmidt, The parasite-specific trypanothione metabolism of trypanosoma and leishmania, Biol. Chem. 384 (4) (2003).
[28] A.H. Fairlamb, Metabolism and functions of trypanothione in the kinetoplastida, Annu. Rev. Microbiol. 46 (1992) 695–729.

[29] Carsten Berndt, Cristopher Horst Lillig, Redox regulation of differentiation and de-differentiation, CRC Press,, 2022.
[30] C. Eichenberger, et al., The highly diverged trypanosomal MICOS complex is organized in a nonessential integral membrane and an essential peripheral module, Mol. Microbiol. (2019) mmi.14389.
[31] I. Kaurov, M. Vancová, B. Schimanski, L.R. Cadena, J. Heller, T. Bílý, D. Potěšil, C. Eichenberger, H. Bruce, S. Oeljeklaus, B. Warscheid, Z. Zdráhal, A. Schneider, J. Lukeš, H. Hashimi, The diverged trypanosome MICOS complex as a hub for mitochondrial cristae shaping and protein import, Curr. Biol. 28 (21) (2018) 3393–3407.e5.
[32] H. Hashimi, A parasite's take on the evolutionary cell biology of MICOS, PLoS Pathog. 15 (12) (2019), e1008166.
[33] J.-F. Collet, J. Messens, Structure, function, and mechanism of thioredoxin proteins, Antioxid. Redox Signal. 13 (8) (2010) 1205–1216.
[34] G. Hofhaus, J.-E. Lee, I. Tews, B. Rosenberg, T. Lisowsky, The N-terminal cysteine pair of yeast sulfhydryl oxidase Erv1p is essential for in vivo activity and interacts with the primary redox centre, Eur. J. Biochem. 270 (7) (2003) 1528–1535.
[35] M.R. McAllaster, A.N. Sinclair-Davis, N.A. Hilton, C.L. de Graffenried, A unified approach towards Trypanosoma brucei functional genomics using Gibson assembly, Mol. Biochem. Parasitol. 210 (1–2) (2016) 13–21.
[36] H. Loferer, M. Wunderlich, H. Hennecke, R. Glockshuber, A bacterial thioredoxin-like protein that is exposed to the periplasm has redox properties comparable with those of cytoplasmic thioredoxins, J. Biol. Chem. 270 (44) (1995) 26178–26183.
[37] J. Haugstetter, T. Blicher, L. Ellgaard, Identification and characterization of a novel thioredoxin-related transmembrane protein of the endoplasmic reticulum, J. Biol. Chem. 280 (9) (2005) 8371–8380.
[38] Y. Sato, K. Inaba, Disulfide bond formation network in the three biological kingdoms, bacteria, fungi and mammals: cellular network for disulfide bond formation, FEBS J. 279 (13) (2012) 2262–2271.
[39] F.E. Dailey, H.C. Berg, Mutants in disulfide bond formation that disrupt flagellar assembly in Escherichia coli. PNAS 90 (3) (1993) 1043–1047.
[40] B. Grumbt, V. Stroobant, N. Terziyska, L. Israel, K. Hell, Functional characterization of Mia40p, the central component of the disulfide relay system of the mitochondrial intermembrane space, J. Biol. Chem. 282 (52) (2007) 37461–37470.
[41] A. Hiniker, J.C.A. Bardwell, In vivo substrate specificity of periplasmic disulfide oxidoreductases, J. Biol. Chem. 279 (13) (2004) 12967–12973.
[42] H. Kadokura, Snapshots of DsbA in action: detection of proteins in the process of oxidative folding, Science 303 (5657) (2004) 534–537.
[43] M. Depuydt, S.E. Leonard, D. Vertommen, K. Denoncin, P. Morsomme, K. Wahni, J. Messens, K.S. Carroll, J.F. Collet, A periplasmic reducing system protects single cysteine residues from oxidation, Science 326 (5956) (2009) 1109–1111.
[44] R.B. Freedman, Native disulphide bond formation in protein biosynthesis: evidence for the role of protein disulphide lsomerase, Trends Biochem. Sci. 9 (1984) 438–441.
[45] F. Hatahet, L.W. Ruddock, Protein disulfide isomerase: a critical evaluation of its function in disulfide bond formation, Antioxid. Redox Signal. 11 (11) (2009) 2807–2850.
[46] M.C.A. Laboissière, S.L. Sturley, R.T. Raines, The essential function of protein-disulfide isomerase is to unscramble non-native disulfide bonds, J. Biol. Chem. 270 (47) (1995) 28006–28009.
[47] V. Peleh, F. Zannini, S. Backes, N. Rouhier, J.M. Herrmann, Erv1 of Arabidopsis thaliana can directly oxidize mitochondrial intermembrane space proteins in the absence of redox-active Mia40, BMC Biol. 15 (1) (2017) 106.
[48] P. Kritsiligkou, A. Chatzi, G. Charalampous, A. Mironov, C.M. Grant, K. Tokatlidis, Unconventional targeting of a thiol peroxidase to the mitochondrial intermembrane space facilitates oxidative protein folding, Cell Rep. 18 (11) (2017) 2729–2741.
[49] G.L. Turra, L. Liedgens, F. Sommer, L. Schneider, D. Zimmer, J. Vilurbina Perez, S. Koncarevic, M. Schroda, T. Mühlhaus, M. Deponte, *In* vivo structure-function analysis and redox interactomes of leishmania tarentolae Erv, Microbiol. Spectr. 9 (2021) e0080921.
[50] S. Alsford, D.J. Turner, S.O. Obado, A. Sanchez-Flores, L. Glover, M. Berriman, C. Hertz-Fowler, D. Horn, High-throughput phenotyping using parallel sequencing of RNA interference targets in the African trypanosome, Genome Res. 21 (6) (2011) 915–924.
[51] T. Bílý, S. Sheikh, A. Mallet, P. Bastin, D. Pérez-Morga, J. Lukeš, H. Hashimi, Ultrastructural changes of the mitochondrion during the life cycle of *Trypanosoma brucei*, J. Eukaryot. Microbiol. 68 (3) (2021).
[52] A. Zíková, Z. Verner, A. Nenarokova, P.A.M. Michels, J. Lukeš, A paradigm shift: the mitoproteomes of procyclic and bloodstream trypanosoma brucei are comparably complex, PLoS Pathog. 13 (12) (2017), e1006679.
[53] V.P. Alibu, L. Storm, S. Haile, C. Clayton, D. Horn, A doubly inducible system for RNA interference and rapid RNAi plasmid construction in Trypanosoma brucei, Mol. Biochem. Parasitol. 139 (1) (2005) 75–82.
[54] D.G. Gibson, L. Young, R.-Y. Chuang, J.C. Venter, C.A. Hutchison, H.O. Smith, Enzymatic assembly of DNA molecules up to several hundred kilobases, Nat. Methods 6 (5) (2009) 343–345.
[55] J.R. Wiśniewski, P. Ostasiewicz, M. Mann, High recovery FASP applied to the proteomic analysis of microdissected formalin fixed paraffin embedded cancer tissues retrieves known colon cancer markers, J. Proteome Res. 10 (7) (2011) 3040–3049.
[56] Y.-G. Yeung, E. Nieves, R.H. Angeletti, E.R. Stanley, Removal of detergents from protein digests for mass spectrometry analysis, Anal. Biochem. 382 (2) (2008) 135–137.
[57] G. Volohonsky, et al., Tools for anopheles gambiae transgenesis, G3 Genes=Genomes|Genet. 5 (6) (2015) 1151–1163.
[58] H.C. Hawkins, M. de Nardi, R.B. Freedman, Redox properties and cross-linking of the dithiol/disulphide active sites of mammalian protein disulphide-isomerase, Biochem. J. 275 (2) (1991) 341–348.
[59] I.S. Arts, G. Ball, P. Leverrier, S. Garvis, V. Nicolaes, D. Vertommen, B. Ize, V. Tamu Dufe, J. Messens, R. Voulhoux, J.F. Collet, Dissecting the machinery that introduces disulfide bonds in *Pseudomonas aeruginosa*, mBio 4 (6) (2013) e00912–e00913.
[60] H. Lu, J. Woodburn, Lu H, Woodburn J. Zinc binding stabilizes mitochondrial Tim10 in a reduced and import-competent state kinetically. J. Mol. Biol. 353 (2005) 897–910.
[61] H.L. Tienson, D.V. Dabir, S.E. Neal, R. Loo, S.A. Hasson, P. Boontheung, S.K. Kim, J.A. Loo, C.M. Koehler, Reconstitution of the Mia40-Erv1 oxidative folding pathway for the small tim proteins, Mol. Biol. Cell 20 (15) (2009) 3481–3490.